Buckling and free vibration behavior of cenosphere/epoxy syntactic foam sandwich beam with natural fibre fabric composite facings under mechanical load

Sunil Waddar[1], Jeyaraj Pitchaimani[1,*], Mrityunjay Doddamani[1], Ever Barbero[2]
[1]Department of Mechanical Engineering, National Institute of Technology Karnataka, Surathkal, India
[2] Mechanical and Aerospace Engineering, West Virginia University Morgantown, WV, 26506-6106, USA
DOI: 10.1016/j.compositesb.2019.107133

Abstract

An experimental study of buckling and dynamic response of cenosphere reinforced epoxy composite (syntactic foam) core sandwich beam with sisal fabric/epoxy composite facings under compressive load is presented. Influence of cenosphere loading and surface modification on critical buckling load and natural frequencies of the sandwich beam under compressive load is presented. The critical buckling load is obtained from the experimental load-deflection data while natural frequencies are obtained by performing experimental modal analysis. Results reveal that natural frequencies and critical buckling load increase significantly with fly ash cenosphere content. It is also observed that surface modified cenospheres enhance natural frequencies and critical buckling load of the sandwich beam under compressive load. Vibration frequencies reduce with increase in compressive load. Fundamental frequency increases exponentially in post-buckling regime. Experimentally obtained load-deflection curve and natural frequencies are compared with finite element analysis wherein results are found to be in good agreement.

Keywords: Sandwich beam, Syntactic foam, Natural fibre fabric, Buckling, Free vibration

1 Introduction

Sandwich composites with lightweight core find applications in marine, wind energy, aerospace and civil engineering structures due to their lower specific weights. Utilising low

* Corresponding author. Email: pjeyaemkm@gmail.com, Phone: +91 77958 58559

strength honeycomb cores or foams, than the metallic honeycomb core helps in reducing weight, manufacturing processes and resources [1]. Sandwich composites comprises of two thin and stiff skins with thick and lightweight core materials stacked in sequence as skin-core-skin. Syntactic foams are a type of closed cell foams wherein closed porosity is present in the microstructure. Syntactic foams are two-component composite material system where hollow spheres are embedded into the matrix resin [2]. Syntactic foams are used as cores in sandwich structures owing to their high specific strength coupled with lower density. The weakest point of the sandwich structures when subjected to different loading conditions is debonding (delamination) of skins from the core material and wrinkling of the compressed side skins under compressive loads [3, 4]. This motivates the researchers to adopt different processing routes for making cost-effective sandwich structures.

Natural fibers are low cost fibers with low density that possess properties comparable to those of man-made synthetic fibers [5, 6]. Natural fiber composites find application in automotive, civil and footwear industries [7, 8]. The commercial use of naturally available sisal fiber reinforced in polymer matrix composites are increasing due to its strength, low density, environmental friendliness and cost effectiveness [9, 10]. Tensile, flexural and dielectric properties of vakka, banana, bamboo and sisal fiber reinforced polymer based composites reveal superior properties as a function of volume fraction. Sisal fiber reinforced polyester composites show higher specific flexural properties compared to the other fibers [11]. Venkateshwaran et al. [12] investigated mechanical and water absorption properties of banana/sisal fiber reinforced with epoxy resin. They observed that sisal fiber reinforced composites exhibited lower water absorption than banana fiber reinforced composites. Among different natural fibres, sisal fibre appears to be promising as they possess higher tensile strength than banana, silk, coir and cotton fibers [5, 13]. The effect of gauge length (10 to 60 mm) on the sisal fiber are reported and found that the elastic modulus increases with gauge

length with insignificant change in tensile strength [14]. Towo and Ansell [15] reported fracture and Dynamic Mechanical Analysis (DMA) of untreated and Sodium hydroxide treated sisal fiber reinforced with polyester and epoxy resin. They observed that the fiber content and fiber treatment enhanced the properties due to increased stiffness and proper interfacial bonding between the constituents. Mechanical properties of sisal-jute-glass fiber reinforced polyester composites are investigated by Ramesh et al. [16]. Their results reveal that jute-sisal mixed with glass fiber reinforced composites show increased flexural strength, whereas sisal fiber mixed with glass fiber reinforced composites presented higher impact strength. Li et al. [17] investigated tensile, flexural and DMA of sisal fiber reinforced in polylactide resin using injection moulding. They reported that the surface modified sisal fiber polylactide composites offered superior properties than untreated ones.

Studies on syntactic foam sandwich composites are available in literature wherein majority of research is focused on mechanical characterisation of foams and their sandwiches. Islam and Kim [18] investigated tensile and flexural response of sandwich composites prepared with paper skin and syntactic foam core. They observed that syntactic foams synthesized with lower particle size exhibits higher flexural properties than the sandwich with higher particle size. John et al.[19] investigated tensile and compressive properties of glass-microballoon/cyanate ester syntactic foam with carbon-cyanate ester skin and observed that the mechanical properties increases with resin content. Analytical approach to evaluate the buckling load of sandwich made of glass/carbon and boron fiber laminate skin and Poly Vinyl Chloride (PVC) foam is established by Aiello and Omres [20]. The theoretical model predicted better global buckling behaviour of sandwich panels for lower values of skin ratio thickness to overall sandwich thickness. Gupta et al. [21] investigated compressive properties of glass microballoon reinforced syntactic foam core with glass-epoxy and glass-carbon-epoxy skins. They observed delayed crack initiation for glass-carbon/epoxy hybrid skin than glass/epoxy ones. Recently

waddar et al. [22, 23] investigated buckling and vibration (free) behavior of cenosphere embedded epoxy (syntactic foams) in bulk form and found that these properties show increasing trend with cenosphere content.

Buckling and free vibration studies of syntactic foam sandwich composites are scarce. Gonclaves et al.[24] investigated numerically buckling and free vibration of PVC foam core sandwich with steel face sheets using coupled stress finite element method. Microstructure dependent beam element predicted more accurate results than the classical Timoshenko beam model. Fleck and Sridhar [25] carried out experimental investigations on sandwich columns made of woven glass fibre epoxy skins and PVC foams with different densities. They observed that the columns undergo different types of buckling phenomenon (Euler macrobuckling, shear microbucking and face microbuckling) depending on the geometry of the sandwich columns. Grognec and Soaud [26] investigated numerically the elastoplastic buckling behaviour of sandwich beams with symmetric homogenous and isotropic core/skin layers subjected to axial compression. The results obtained numerically are in good agreement with the available analytical solutions. Grygorowicz et al.[27] presented analytical and numerical buckling analysis of sandwich columns with aluminium face sheet and aluminium alloy foam core. Mathieson et al. [28] investigated experimentally the effect of cross-sectional configuration and slenderness ratio on GFRP skin and polyurethane core sandwich composites. Lower slenderness ratios resulted in skin wrinkling mode of failure and length greater than critical slenderness ratios resulted in global buckling. Jasion and Magnucki [29] performed experimental, analytical and numerical analysis on buckling behaviour of aluminium foam core sandwich with aluminium face sheet subjected to axial compressive load. Experimentally obtained critical buckling loads are found to be closer to analytical and numerical results. Salleh et al. [30] investigated experimentally the mechanical properties of GFRP/vinyl ester skin with glass microballoon/vinyl ester syntactic foam core sandwich panels. They found that the

properties are dependent on the weight fraction of the glass microballoons, void content and interfacial bonding between the constituents. Smyczynski and Magnucka-Blandzi [31] analysed buckling behaviour of simply supported sandwich beam with aluminium face and foam core numerically using transverse shear deformation effect. Sokolinsky et al.[32] investigated free vibration response of polymer foam core and steel face sheet cantilever sandwich beam analytically and experimentally. The results obtained using higher order theory are found to be in good agreement with experimental values. Tang et al.[33] investigated buckling behaviour of fixed-fixed and hinged-hinged calcium silicate face sheets sandwich panels with polyurethane foam core subjected to axial load. Buckling load values obtained through analytical, numerical (finite element method) and experimental routes matches closely. Wu et al. [34] investigated numerically the buckling and free vibration response of functionally graded carbon nanotube (CNT) reinforced composite face sheets with Titanium alloy core using Timoshenko beam theory. They observed that CNT volume fraction, end supporting conditions and slenderness ratio have significant influence on critical buckling loads and natural frequencies.

Literature review suggests that the sisal fiber reinforced skins with fly ash cenospheres reinforced in polymer matrix core should be explored for sandwich construction owing to higher specific properties finding applications in aerospace and marine industries. Main objective of the present work is to investigate buckling and dynamic behavior of sandwich beam with fly ash cenosphere/epoxy as core with sisal fibre fabric composite laminate facings under compressive load. Effect of fly ash cenospheres loading and its surface modification on critical buckling load and free vibration frequencies of the sandwich beam under compressive load is studied in detail. Elastic properties of fly ash cenosphere and sisal fabric reinforced epoxy laminate are obtained experimentally. These values are further used to predict the critical

buckling load and free vibration frequencies numerically. Finally, the numerical and experimental results are compared.

2 Constituent materials and methodologies

2.1 Constituent materials

LAPOX L-12 Epoxy resin and K-6 hardener, both acquired from Atul Ltd., Gujarat is used to prepare syntactic foam cores and their skin. Sisal natural fibre fabric woven in plain architecture procured from Jolly Enterprise, Kolkata is used as reinforcement as sandwich facing. Cenospheres of grade CIL-150 (Cenosphere India Pvt Ltd., Kolkata) is used as filler for core. Cenospheres are hollow in nature, spherical in shape and have Al_2O_3, SiO_2, CO and Fe_2O_3 as the major constituents [23, 35, 36]. 3-Amino Propyl tri ethoxy silane treated and untreated (as received) cenospheres/epoxy syntactic foams are prepared and used as cores for sandwich. The procedure for surface treatment and silane coating confirmatory tests are outlined in Ref. [22].

2.2 Syntactic foam preparation

Untreated (as received) and silane treated cenosphere/epoxy syntactic foam sandwich cores are prepared with varying volume fraction (20, 40 and 60%) in epoxy resin. Predetermined quantity of cenospheres and epoxy resin are weighed and homogenous slurry is formed using manual stirring method. K6 hardener (10 wt.%) is added to initiate polymerization in the cenosphere/epoxy slurry before decanting it into the aluminium mold. For easy sequestration of foam slabs from the mold, silicone is smeared through. Curing time of 24 hours at room temperature is maintained through for all the samples including sandwiches. The syntactic foams are then polished to the thickness of 2.5 mm using belt polishing machine with grit size of 120 and later cleaned using acetone. All prepared syntactic foams are named as $E_{XX}Y$ (E - pure epoxy resin, $_{XX}$ – filler loading, Y - untreated [U]/treated [T]).

2.3 Sandwich construction

Sandwich composites are prepared using hand lay-up process. Initially the skins/facings are wetted using epoxy matrix and excess epoxy from the skin is removed. The wetted skins of desired thickness are laid on the bottom plate of the mold and foam core of known thickness is placed on top of bottom skin. Later, wetted skin is placed on top of the core. The upper plate is placed on the top of upper skin and clamped firmly (Figure 1) to maintain overall sandwich thickness of 4 mm. The specimens for the testing are cut from the cast sandwich panels using diamond saw cutter. Sandwiches prepared are represented by $S_{EXX}Y$ (S - sisal/epoxy facing).

2.4 Density test

ASTM D792-13 is employed to find experimental densities of syntactic foams and their sandwiches. Results of five replicates of foams and their sandwiches are presented in Table 1 and Table 2 respectively. Rule of mixtures (Equation 1) is adopted to compute theoretical densities of syntactic foams and sandwich composites.

$$\rho^{th} = \rho_m V_m + \rho_f V_f \tag{1}$$

where, ρ, V, f and m denote density, volume fraction, filler and matrix respectively. Void content (ϕ_v) in the samples is calculated by taking relative difference between theoretical (ρ^{th}) and experimentally measured (ρ^{exp}) density [37].

$$\phi_v = \frac{\rho^{th} - \rho^{exp}}{\rho^{th}} \tag{2}$$

2.5 Buckling test

Universal Testing Machine (H75KS, Tinius Olsen make, UK) with maximum loading capacity of 50 kN is used to perform the tests with cross-head displacement rate constant at 0.2 mm/min. Five sandwich specimens having dimension of 210 × 12.5 × 4 mm are subjected to compressive load. Schematics of the test setup is shown in Figure 2. The deflection behavioural changes of

sandwich beams subjected to axial compression in pre and post buckling regime are observed by keeping the constant end shortening limit as 0.75 mm. Graphical methods (DTM - double tangent method, MBC - Modified Budiansky criteria) are used to determine critical buckling load (P_{cr}) from experimentally acquired data of load and deflection [38, 39]. DTM uses two tangents drawn to load-deflection curve in the pre and post-buckling regimes. The point of intersection of the two tangents is considered as critical buckling load. In MBC the bisector point of the two tangents drawn to load-deflection curve is considered as the critical buckling load [22].

2.6 Free vibration test at no load and axial compression

Modal analysis through experimental route is employed to envisage fundamental frequencies pertaining to first three bending modes of sandwiches under clamped-clamped boundary condition. Schematic representation of experimental setup is presented in Figure 2. The sandwich beams are excited using an impulse hammer and vibration responses are acquired using a uniaxial type accelerometer. Kistler make impulse hammer (Model:9722A2000) having sensitivity of 10mV/N and light weight Kistler accelerometer (Model: 8778A500) with sensitivity of 10mV/g having operating range of ± 500g are used. Bee's wax is applied on specimen for better adhesion with accelerometer. The input excitation and vibration response signals acquired from accelerometer are fed into DEWE Soft software, where Fast Fourier Transform (FFT) algorithm is use to convert time to frequency domain signals, yielding to natural frequencies and mode shapes. The test is repeated at every incremental load of 50N. Compressive load is temporarily paused for 2 minutes to accomplish the modal analysis of the syntactic foam sandwich under compressive load.

2.7 Evaluation of Elastic Properties of Skin

Elastic properties associated with cenosphere/epoxy syntactic foam cores and sisal fabric/epoxy facing are estimated experimentally. These properties are further used to calculate

the critical buckling load and free vibration frequencies of the sandwich beam using finite element based numerical approach. Elastic properties of the cenosphere/epoxy syntactic foam core are estimated based on Bardella-Genna model and are presented in our previous work [22]. In order to estimate the skin properties, fiber properties such as tensile strength and Young's modulus of sisal yarn are found by performing tensile test as per ASTM D3822-16 on six samples. Cross head movement is maintained constant at 5 mm/min. Yarn specimen with diameter 0.5 mm and gauge length of 50 mm (Figure 3) are also tensile tested. Elastic properties of sisal fabric/epoxy composite skin materials are estimated according to the procedure as outlined in Ch.9 of Ref.[40]. The tensile (Type I), compressive and flexural properties of epoxy matrix are estimated using ASTM D638-15, ASTM D695-16 and ASTM D790-16 respectively. Tensile, compression and flexural tests are carried out with the cross-head displacement speed at 5, 1.4 and 1.3 mm/min respectively. Specimens dimension of 127×12.7×3.2 mm and 12.7× 12.7×25.4 mm are used for estimating flexural and compressive properties.

The microstructural geometry of the fabric is presented in Figure 4. The geometrical parameters of fabric are given as, Fill width $a_f = \frac{1}{N_f}$, warp width $a_w = \frac{1}{N_w}$, where, N_f and N_w are number of yarns per unit width in fill and warp directions respectively. If number of yarns along warp and fill directions are the same then $N_f = N_w$ condition prevails. In this case fill thickness (h_f) and warp thickness (h_w) are equal to half of lamina thickness (h). Harness (n_g) is the number of yarns along fill or warp direction of the representative unit cell. Shift (n_s) is the number of yarns between two consecutive interlaced regions. Interlacing (n_i) is the number of yarns in the interlaced region. All these parameters define the representative volume element of the fabric reinforced laminate. Based on these values, further moduli of the laminate are computed.

The sisal fabric used in the present work is woven with plain weaving architecture. Fabric being square in symmetry, number of yarns per unit length in fill and warp direction is constant. Hence the transverse modulus is equal to longitudinal modulus (i.e. $E_x = E_y$).The longitudinal modulus (E_x) of a sisal /epoxy tow is calculated using rule of mixtures and is given by,

$$E_x = E_m V_m + E_f V_f \tag{3}$$

where, E is Young's modulus, V is volume fraction and suffices *m* and *f* represents matrix and fiber respectively.

Longitudinal and transverse Poisson's ratios are calculated using the relation,

$$\vartheta_{12} = \vartheta_{23} = \vartheta_m V_m + \vartheta_f V_f \tag{4}$$

In-plane shear, modulus is computed using periodic microstructure micromechanics (PMM) [40] and is given by,

$$G_{12} = G_m \left[1 + \frac{V_f \left(1 - \frac{G_m}{G_f} \right)}{\frac{G_m}{G_f} + S_3 \left(1 - \left(\frac{G_m}{G_f} \right) \right)} \right] \tag{5}$$

where,

$$S_3 = 0.49247 - 0.47603 V_f - 0.02748 V_f^2 \tag{6}$$

Interlaminar shear modulus is calculated using PMM [41] formula and is given by,

$$G_{23} = G_m - \frac{V_f}{D} \tag{7}$$

where, D is constant and is given by,

$$D = \frac{(2G_m + C'_{23} - C'_{22})(4S_7 - 2(2 - 2\vartheta_m)S_3) + 2G_m(2 - 2\vartheta_m)}{G_m(2G_m + C'_{23} - C'_{22})(2 - 2\vartheta_m)} \tag{8}$$

$$C'_{22} = \left(1 - \vartheta_f^2\right) \frac{E_f}{\Delta} \tag{9}$$

$$C'_{23} = \left(\vartheta_f + \vartheta_f^2\right)\frac{E_f}{\Delta} \quad (10)$$

where, $\Delta = 1 - \vartheta_f^2 - 2\vartheta_f^3$ (11)

$$S_7 = 0.12346 - 0.32035V_f - 0.23517V_f^2 \quad (12)$$

Computer aided design environment for composites (CADEC) [42] is used to find the properties of sisal fabric/epoxy skin which are then used to model the skin of the sandwich beam. Figure 5 shows the methodology followed to compare experimental and numerical results. The Bardella-Genna model (BGM) is used to estimate the properties of the core. BGM uses homogenisation approach and calculates the elastic properties of foams based on volume fraction and radius ratio as explained in Ref. [22].

The sandwich beam is modelled as a layered structure using four noded, "SHELL 181", element available in ANSYS. A rectangle of size 210×12.5 mm is created to represent the geometry of the sandwich beam. Sandwich skin and core are modelled as orthotropic and isotropic materials. Material properties of core and skin materials are specified for the respective layers. The geometry is meshed with 50 "SHELL181" elements. Displacement boundary conditions and loads are applied. ANSYS is used to perform buckling and vibration analysis.

2.8 Finite Element Analysis

The fundamental buckling mode of the sandwich beam is obtained from the linear Eigen value analysis. Further, non-linear static structural analysis (Newton-Rapson method) is conducted by incorporating geometric imperfections in the model. The geometrical imperfection shape and amplitude is chosen based on trial and error method to obtain close match with experimental and numerical results is obtained. The structural stiffness matrix ($[K]$) is given by,

$$[K] = \int [B]^T [D][B] dV \quad (13)$$

where, $[B]$ and $[D]$ are linear strain-displacement and constitutive matrices respectively. The effect of axial compressive load in the numerical analysis and pre-stress effect on the structure are considered by the stress stiffness matrix ($[K_\sigma]$)

$$[K_\sigma] = \int_V [B_d]^T [S][B_d] \, dV \quad (14)$$

where $[K_\sigma]$ and $[B_d]$ represents stress stiffness and strain-displacement matrix respectively, [S] represents pre-stress matrix due to the axial compressive load.

$$[S] = \begin{bmatrix} \sigma_x & \sigma_{xy} \\ \sigma_{xy} & \sigma_y \end{bmatrix} \quad (15)$$

where, σ_x, $\sigma_{xy,}\sigma_y$ are membrane forces generated in the structure due to the axial compressive load. Further, linear eigenvalue buckling analysis is completed using the structural and stress stiffness matrices and as follows

$$([K] + \lambda_i[K_\sigma])\{\psi_i\} = 0 \quad (16)$$

where, λ is buckling load, ψ represent mode shape and i is the mode number. Equation 16 estimates buckling load and fundamental mode shape, which is used in non-linear static analysis as follows,

$$[K(u)]\{u\} = \{F\} \quad (17)$$

where, [K(u)] represents tangent stiffness matrix and 'F' is the load in each sub-step in Newton-Raphson method. The total load is subdivided into a series of increments and is applied over several sub-steps. The maximum load considered for nonlinear analysis is P_{cr} obtained from linear buckling analysis. The outcome of Equation 17 is a load-deflection curve based on numerical simulations which then is compared with experimental results.

The experimentally obtained first three natural frequencies of the sandwich beam in absence of axial compressive load are compared with numerical results. Modal analysis is carried out to extract the first three natural frequencies. The natural frequencies are calculated by solving the following Eigen value problem,

$$([K] - \omega_i{}^2[M])\{\phi_i\} = 0 \quad (18)$$

where, $[K]$ is the stiffness matrix, $[M]$ structural mass matrix, $\{\phi_i\}$ is corresponding mode shape and ω represents the natural frequency.

3 Results and discussion

3.1 Material characterization

Cores of sandwich are made of untreated (as received) and silane treated cenospheres reinforced in epoxy matrix. Figure 6a represents micrograph of untreated cenosphere/epoxy composite where numerous defects are seen on the exterior cenosphere surface. Sphericity variations and numerous defects on the surface change the surface morphology and may lead to deviations from the theoretically predicted values. Micrograph of silane treated cenosphere is presented in Figure 6b. Though the silane coating layer is not clearly visible from the micrograph, FTIR spectrum showed 3-aminopropyl tri ethoxy silane peak around 2929 cm^{-1} on treated cenospheres confirming silane coating on cenospheres [43, 44]. Particle size analysis revealed increase in mean particle size for treated cenospheres. Weighted average median of treated and untreated fly ash cenospheres is 55.08 and 48.24 µm respectively [22]. The density of treated and untreated cenospheres are 1000 and 920 kg/m^3 respectively [22, 35, 36]. Surface modification of cenosphere leads to increase in density of particle by 8.69 %, however it is less than the epoxy resin (1184.54 kg/m^3) indicating possibility of weight reduction.

Experimentally density of sisal fibres is found according to ASTM D3800-16. Sisal yarn specimens of length 1 m are tested. Ten replicates are tested and average values are reported. The density of sisal fibers is found to be 1262.80 ± 46.23 kg/m^3.

It is a challenging task to synthesize syntactic foams with uniform cenosphere dispersion in the matrix, minimizing particle breakage and cluster formation while processing. Quality and mechanical behaviour of samples is dependent on cenospheres survival and void content. As cast micrographs of $E_{60}U$ syntactic foams is presented in Figure 6c at low magnification. Uniform distribution of cenospheres in the matrix resin is clearly evident from the micrograph. Clusters of cenospheres are not seen in the $E_{60}U$ sample as observed from Figure 6c.

Sandwich composites with sisal fabric/epoxy as skin and fly ash syntactic foam as cores are prepared by hand lay-up process as described in section 2.3. Figure 7 shows schematic representation of the sandwich beam and prepared sandwich sample. Figure 8 represent micrograph of sandwich composite post freeze fracture. Distinct region of skin indicating firm bonding and core materials is observed from Figure 8. Further, both top and bottom skin thickness is uniformly maintained with a thickness of around 0.75 mm (Figure 8b). Small variation of ± 0.1mm is observed in skin thickness is attributed to undulation of the woven fabric. Absence of voids indicate sound quality of sandwich samples without skin delamination from the core.

3.2 Density of syntactic foams

Quality and properties of syntactic foams and their sandwich composites are depending upon the amount of intact hollow particles and void volume. Presence of air entrapment during mechanical mixing of fly ash cenospheres in epoxy resin and hand lay-up process during sandwich preparation is accounted for void content. Table 1 and Table 2 represent density and

void content results of foams and their sandwiches respectively. Theoretical densities (Equation 1) are found to be higher as compared to experimental values (Table 1 and Table 2). Lower experimental densities compared to theoretical densities are due to air entrapment owing to cenospheres mechanical mixing in the resin for syntactic foam cores and in sandwich facings.

Few voids as evident from Figure 6c is seen in representative $E_{60}U$ foam sample which and is a syntactic foams typical feature. These voids are undesirable from mechanical properties perspective. From Table 1, it is observed that void content in syntactic foams increases with cenosphere content. Maximum void content is observed for $E_{60}T$ is 5.58% indicating good quality samples. Density of as received and treated cenosphere reinforced epoxy decreases in the range of 6.43-15.81 and 5.67-14.61% (Table 1) respectively. Densities of surface modified cenosphere syntactic foams are higher than untreated ones owing to higher mean particle size in surface modified cenospheres. Densities (theoretical and experimental) of cenosphere/epoxy syntactic foam sandwich with sisal/epoxy skin is presented in Table 2. From Table 2, it is noted that the density of sandwich composites decrease with increase in cenosphere loading in the core material and the void volume is in the narrow range of 0.91-4.54% (Figure 8).

3.3 Buckling behaviour

Sandwich beams are subjected to axial compressive load using universal testing machine with clamped-clamped condition (Figure 2). The axial compressive load applied and deflection along the beam axis is recorded using data acquisition system.

The buckling load of sandwich composites increases as a function of cenosphere loading (Figure 9 and Table 3). This is attributed to addition of stiffer cenospheres increase the overall foam stiffness. Presence of woven sisal fiber fabric skin renders additional stiffness to the beam. During the test the sandwich beams exhibit global buckling mode and maximum

deflection is observed at the mid portion of the beam as depicted by Figure 10b. There are no signs of skin wrinkling and skin microbuckling as evident from Figure 10b. This can be attributed to the lesser amount of axial compressive stresses developed in the skins as compared to skin plastic microbuckling and wrinkling strength [25].

The most common mode of failure associated with sandwich structures is skin delamination which is seen to be absent for all the samples indicating good adhesive strength between the skin and core. In Table 3, $S_{EXX}T$ beams have higher buckling loads than $S_{EXX}U$ ones. Silane treated cenospheres in epoxy resin enhances the elastic modulus due enhanced interfacial bonding between the constituents increasing overall stiffness of the foams. Increase in mean particle size due to silane treatment also augments foams stiffness enabling them for structural applications. The buckling load increase in the range of 7.86-25.44% and 19.92-38.99% respectively for untreated and treated syntactic foam sandwich composites as compared to neat epoxy core sandwich. Critical buckling load estimates by DTM and MBC techniques match very closely (within 1%) as seen from Table 3.

Table 4 presents comparison of buckling loads of cenosphere/epoxy syntactic foams and the sandwich beams tested in present study. It can be observed from Table 4 that the buckling loads of the sandwich beams are higher (7.32- 55.72%) than the syntactic foam for the same sample dimensions subjected to similar testing conditions. Such an increment can be attributed to enhanced stiffness due to sisal/epoxy skins in sandwich beams. Change in stiffness due to axial compressive loads influences dynamic properties, particularly natural frequency necessitating their estimates.

3.4 Free vibration behaviour at no load and axial compression

Modal analysis through experimental route is performed to find natural frequencies pertaining to first three transverse bending mode shapes of the sandwich beam. DEWE Soft® software is

used for converting time into frequency domain (Frequency response functions) signals using FFT algorithm. Further, experimental natural frequencies are validated with numerical results obtained through finite element method.

Table 5 depicts first 3 natural frequencies of the sandwich beams in clamped-clamped condition at no load condition. Natural frequencies of sandwich beam increases with cenosphere volume. The increase in natural frequency might be due to higher composite stiffness (stiff cenosphere in the matrix) and also due to surface modified intact cenospheres (in treated cenosphere/epoxy syntactic foams). Thereby the natural frequencies of the sandwich composites with treated syntactic foam cores are higher as compared to untreated syntactic foam core sandwiches for all the filler loadings (Figure 11). Increasing compressive load decreases natural frequency. Fundamental natural frequency of sandwich beams reaches minimum value when the load approaching towards critical buckling load and increases rapidly after passing critical buckling load due to higher stiffness because of beams deflection (Figure 11a). Similar trend is observed in previous studies [22, 34, 45, 46] of isotropic/composites beam and columns. Fundamental natural frequency drops suddenly at the closer point of critical buckling load which leads to lower structural stiffness values (Figure 11a). The syntactic foam modulus increases with increase in filler content. Further, stiffness of the sandwich composite increases owing to the woven natural fiber reinforced epoxy skin. Volume fraction of the natural fiber used as skin in sandwiches is approximately the same for the tested samples. Thereby, natural frequencies enhancement is solely attributed to the filler loading.

3.5 Comparison of experimental and numerical buckling and free vibration results

Figure 12 represents images of sisal fiber, yarn and plain-woven fabric samples used in the present study. The tensile test (Figure 3) of yarn is carried out and the stress-strain response is

plotted in Figure 13. The properties of sisal fiber is listed in Table 6. The tensile strength and modulus of yarn is found to be 255 and 8861.11 MPa respectively. Tensile, compressive and flexural properties of neat epoxy samples are deduced by conducting the tests as outlined in section 2.7. The properties of Epoxy matrix are presented in Table 7. The fabric geometry is measured to obtain the necessary geometric parameters (Figure 4). Different intrinsic fabric lamina properties and geometric parameters obtained for sisal fabric are listed in Table 8. Using the data associated with fiber, epoxy and geometry of fabric, the elastic properties of the skin material are estimated with the help of CADEC [42]. The methodology used by CADEC is explained in Chapter 9 of Ref.[40] Predicted skin properties (CADEC results) are reported in Table 9. Tensile properties of single layer Sisal fabric/epoxy are also compared with CADEC values Table 9. Tensile specimens of dimension 250×25×0.75 mm are prepared and tested at 2mm/min (ASTM D3039-17). Good agreement between CADEC and experimental values are obtained. These properties are further used for numerical analysis to find the natural frequencies of the sandwich beams.

Elastic properties associated with cenosphere/epoxy syntactic foam are obtained using Bardella-Genna model (BGM) and are used as input to finite element analysis. Estimated elastic properties of developed syntactic foams are listed in Table 10. Young's modulus shows increasing trend as filler loading increases, and such effect is more prominent in case of treated cenospheres. Improved interfacial bonding between the constituents plays a crucial role for such an observation.

Elastic properties of the skin material (sisal fabric/epoxy) (Table 9) estimated with CADEC [42] and elastic properties of the (cenosphere/epoxy) core material estimated using BGM (Table 10) are used as an input to numerical analysis using ANSYS. Linear eigen-value buckling analysis is conducted to understand the fundamental buckling mode which is

considered to represent the geometric imperfection. Subsequently non-linear static structural analysis is carried out. Load-deflection responses are graphed to compare experimental values with numerical results. Figure 14 presents comparative plots for $S_{E40}U$ and $S_{E40}T$ sandwich samples. Numerical and experimental buckling loads are presented in Table 11. Maximum deviation is noted to be 18.41% between numerical and experimental buckling results. Numerical simulations predict the load-deflection behavior and buckling load reasonably yet lower than experimental results. Modulus variation is clearly evident from Figure *14*. Numerous surface defects on cenospheres like non-sphericity, variations in shell wall thickness and built-in porosity in the walls might be responsible for the deviations of numerically predicted values from that of experimental results. Accuracy in obtaining skin properties can be improved with more accurate measurements of microstructural properties of fabric as input to CADEC

Modal analysis is carried out to extract first three natural frequencies for sandwiches. Comparison of numerical results with experimental values is presented in Table 12. Experimental and numerical results are in good agreement (within 12.9%). Sandwich composites with sisal/epoxy skin and cenosphere/epoxy cores show better buckling and free vibrations characteristics than sandwiches with neat epoxy core.

Conclusions

Buckling and free vibration response of sisal fabric/epoxy skin and syntactic foam core is investigated experimentally and numerically. The weight saving potential of untreated and treated cenosphere/epoxy syntactic foams is 15.81 and 14.61% respectively as compared to neat samples. The sandwich beams show global buckling mode shape without skin delamination or skin wrinkling. As the filler loading increases, buckling load and natural frequencies are observed to be increasing. These values for sandwich composites with treated cenosphere/epoxy foam core are higher than the untreated cenosphere/epoxy foam sandwich

samples because enhanced stiffness of core due to proper adhesion between the constituents. Further, the natural frequencies decrease with increase of the axial compressive load. The first natural frequency represents minimum value at critical buckling load and later increases exponentially post critical buckling load due to gain in geometrical stiffness of the beam. The skin properties are found using CADEC and are found in good agreement with the experimental values. Further properties obtained from CADEC and Bardella-Genna model are used for numerical analysis. Experimental results are compared with numerically predicted values and are found to be in good agreement.

Acknowledgments

The authors thank the Mechanical Engineering Department at National Institute of Technology Karnataka for providing facilities and support.

References

1. Frostig, Y., *Buckling of sandwich panels with a flexible core—high-order theory.* International Journal of Solids and Structures, 1998. **35**(3): p. 183-204.
2. Gupta, N., S.E. Zeltmann, V.C. Shunmugasamy, and D. Pinisetty, *Applications of Polymer Matrix Syntactic Foams.* JOM, 2014. **66**(2): p. 245-254.
3. Corigliano, A., E. Rizzi, and E. Papa, *Experimental characterization and numerical simulations of a syntactic-foam/glass-fibre composite sandwich.* Composites Science and Technology, 2000. **60**(11): p. 2169-2180.
4. Ji, W. and A.M. Waas, *Global and local buckling of a sandwich beam.* Journal of Engineering Mechanics, 2007. **133**(2): p. 230-237.
5. Pickering, K.L., M.G.A. Efendy, and T.M. Le, *A review of recent developments in natural fibre composites and their mechanical performance.* Composites Part A: Applied Science and Manufacturing, 2016. **83**: p. 98-112.
6. Nabi, S.D. and J.J. P., *Natural fiber polymer composites: A review.* Advances in Polymer Technology, 1999. **18**(4): p. 351-363.
7. Alves, C., P.M.C. Ferrão, A.J. Silva, L.G. Reis, M. Freitas, L.B. Rodrigues, and D.E. Alves, *Ecodesign of automotive components making use of natural jute fiber composites.* Journal of Cleaner Production, 2010. **18**(4): p. 313-327.
8. Verney, J.C.K.d., M.F.S. Lima, and D.M. Lenz, *Properties of SBS and sisal fiber composites: ecological material for shoe manufacturing.* Materials Research, 2008. **11**: p. 447-451.
9. Ibrahim, I.D., T. Jamiru, E.R. Sadiku, W.K. Kupolati, S.C. Agwuncha, and G. Ekundayo, *Mechanical properties of sisal fibre-reinforced polymer composites: a review.* Composite Interfaces, 2016. **23**(1): p. 15-36.
10. Gurunathan, T., S. Mohanty, and S.K. Nayak, *A review of the recent developments in biocomposites based on natural fibres and their application perspectives*. Composites Part A: Applied Science and Manufacturing, 2015. **77**: p. 1-25.
11. Murali Mohan Rao, K., K. Mohana Rao, and A.V. Ratna Prasad, *Fabrication and testing of natural fibre composites: Vakka, sisal, bamboo and banana.* Materials & Design, 2010. **31**(1): p. 508-513.
12. Venkateshwaran, N., A. ElayaPerumal, A. Alavudeen, and M. Thiruchitrambalam, *Mechanical and water absorption behaviour of banana/sisal reinforced hybrid composites.* Materials & Design, 2011. **32**(7): p. 4017-4021.
13. Jacob, M., S. Thomas, and K.T. Varughese, *Mechanical properties of sisal/oil palm hybrid fiber reinforced natural rubber composites.* Composites Science and Technology, 2004. **64**(7): p. 955-965.
14. Alves Fidelis, M.E., T.V.C. Pereira, O.d.F.M. Gomes, F. de Andrade Silva, and R.D. Toledo Filho, *The effect of fiber morphology on the tensile strength of natural fibers.* Journal of Materials Research and Technology, 2013. **2**(2): p. 149-157.
15. Towo, A.N. and M.P. Ansell, *Fatigue evaluation and dynamic mechanical thermal analysis of sisal fibre–thermosetting resin composites.* Composites Science and Technology, 2008. **68**(3): p. 925-932.
16. Ramesh, M., K. Palanikumar, and K.H. Reddy, *Mechanical property evaluation of sisal–jute–glass fiber reinforced polyester composites.* Composites Part B: Engineering, 2013. **48**: p. 1-9.
17. Li, Z., X. Zhou, and C. Pei, *Effect of Sisal Fiber Surface Treatment on Properties of Sisal Fiber Reinforced Polylactide Composites.* International Journal of Polymer Science, 2011. **2011**.

18. Islam, M.M. and H.S. Kim, *Sandwich composites made of syntactic foam core and paper skin: Manufacturing and mechanical behavior.* Journal of Sandwich Structures & Materials, 2012. **14**(1): p. 111-127.
19. Bibin, J., R.N.C. P., M. Dona, and N.K. N., *Foam sandwich composites with cyanate ester based syntactic foam as core and carbon-cyanate ester as skin: Processing and properties.* Journal of Applied Polymer Science, 2008. **110**(3): p. 1366-1374.
20. Aiello, M.A. and L. Ombres, *Buckling Load Design of Sandwich Panels Made with Hybrid Laminated Faces and Transversely Flexible Core.* Journal of Sandwich Structures & Materials, 2007. **9**(5): p. 467-485.
21. Gupta, N. and S. Sankaran, *On the Characterisation of Syntactic Foam Core Sandwich Composites for Compressive Properties.* Journal of Reinforced Plastics and Composites, 1999. **18**(14): p. 1347-1357.
22. Waddar, S., P. Jeyaraj, and M. Doddamani, *Influence of axial compressive loads on buckling and free vibration response of surface-modified fly ash cenosphere/epoxy syntactic foams.* Journal of Composite Materials, 2018: p. 0021998317751284.
23. Waddar, S., J. Pitchaimani, and M. Doddamani, *Snap-through buckling of fly ash cenosphere/epoxy syntactic foams under thermal environment.* Thin-Walled Structures, 2018. **131**: p. 417-427.
24. Reinaldo Goncalves, B., A. Karttunen, J. Romanoff, and J.N. Reddy, *Buckling and free vibration of shear-flexible sandwich beams using a couple-stress-based finite element.* Composite Structures, 2017. **165**: p. 233-241.
25. Fleck, N.A. and I. Sridhar, *End compression of sandwich columns.* Composites Part A: Applied Science and Manufacturing, 2002. **33**(3): p. 353-359.
26. Le Grognec, P. and K. Sad Saoud, *Elastoplastic buckling and post-buckling analysis of sandwich columns.* International Journal of Non-Linear Mechanics, 2015. **72**: p. 67-79.
27. Grygorowicz, M., K. Magnucki, and M. Malinowski, *Elastic buckling of a sandwich beam with variable mechanical properties of the core.* Thin-Walled Structures, 2015. **87**: p. 127-132.
28. Mathieson, H. and A. Fam, *Axial Loading Tests and Simplified Modeling of Sandwich Panels with GFRP Skins and Soft Core at Various Slenderness Ratios.* Journal of Composites for Construction, 2015. **19**(2): p. 04014040.
29. Jasion, P. and K. Magnucki, *Global buckling of a sandwich column with metal foam core.* Journal of Sandwich Structures & Materials, 2013. **15**(6): p. 718-732.
30. Salleh, Z., M.M. Islam, J.A. Epaarachchi, and H. Su, *Mechanical properties of sandwich composite made of syntactic foam core and GFRP skins.* AIMS Materials Science, 2016. **3**(4): p. 1704-1727.
31. Smyczynski, M.J. and E. Magnucka-Blandzi, *Static and dynamic stability of an axially compressed five-layer sandwich beam.* Thin-Walled Structures, 2015. **90**: p. 23-30.
32. Sokolinsky, V.S., H.F. Von Bremen, J.A. Lavoie, and S.R. Nutt, *Analytical and Experimental Study of Free Vibration Response of Soft-core Sandwich Beams.* Journal of Sandwich Structures & Materials, 2004. **6**(3): p. 239-261.
33. Tang, Z., X. Zha, and J. Ma, *Buckling of axially loaded sandwich composite panels with reinforced calcium silicate faces and polyurethane cores.* Journal of Reinforced Plastics and Composites, 2015. **34**(17): p. 1378-1391.
34. Wu, H., S. Kitipornchai, and J. Yang, *Free Vibration and Buckling Analysis of Sandwich Beams with Functionally Graded Carbon Nanotube-Reinforced Composite Face Sheets.* International Journal of Structural Stability and Dynamics, 2015. **15**(07): p. 1540011.

35. Garcia, C.D., K. Shahapurkar, M. Doddamani, G.C.M. Kumar, and P. Prabhakar, *Effect of arctic environment on flexural behavior of fly ash cenosphere reinforced epoxy syntactic foams.* Composites Part B: Engineering, 2018. **151**: p. 265-273.
36. Shahapurkar, K., C.D. Garcia, M. Doddamani, G.C. Mohan Kumar, and P. Prabhakar, *Compressive behavior of cenosphere/epoxy syntactic foams in arctic conditions.* Composites Part B: Engineering, 2018. **135**: p. 253-262.
37. Tagliavia, G., M. Porfiri, and N. Gupta, *Analysis of flexural properties of hollow-particle filled composites.* Composites Part B: Engineering, 2010. **41**(1): p. 86-93.
38. Tuttle, M., P. Singhatanadgid, and G. Hinds, *Buckling of composite panels subjected to biaxial loading.* Experimental Mechanics, 1999. **39**(3): p. 191-201.
39. Matsunaga, H., *Free vibration and stability of thin elastic beams subjected to axial forces* Journal of Sound and Vibration, 1996. **191**(5): p. 917-933.
40. Barbero, E.J., *Introduction to composite materials design*. 3 ed. 2018: CRC press.
41. Barbero, E.J., *Workbook for Introduction to Composite Materials Design*, 3ed. 2018, Create space, South Charleston, NC.
42. CADEC. *websource*, http://en.cadec-online.com. 10 Nov 2018].
43. Kumar, B.R.B., Z.S. Eric, D. Mrityunjay, G. Nikhil, Uzma, G. S., and S.R.R. N., *Effect of cenosphere surface treatment and blending method on the tensile properties of thermoplastic matrix syntactic foams.* Journal of Applied Polymer Science, 2016. **133**(35).
44. Bharath Kumar, B.R., M. Doddamani, S.E. Zeltmann, N. Gupta, Uzma, S. Gurupadu, and R.R.N. Sailaja, *Effect of particle surface treatment and blending method on flexural properties of injection-molded cenosphere/HDPE syntactic foams.* Journal of Materials Science, 2016. **51**(8): p. 3793-3805.
45. Rajesh, M. and J. Pitchaimani, *Experimental investigation on buckling and free vibration behavior of woven natural fiber fabric composite under axial compression.* Composite Structures, 2017. **163**: p. 302-311.
46. Mirzabeigy, A. and R. Madoliat, *Large amplitude free vibration of axially loaded beams resting on variable elastic foundation.* Alexandria Engineering Journal, 2016. **55**(2): p. 1107-1114.
47. da Silva, L.J., T.H. Panzera, A.L. Christoforo, L.M.P. Durão, and F.A.R. Lahr, *Numerical and experimental analyses of biocomposites reinforced with natural fibres.* International Journal of Materials Engineering, 2012. **2**(4): p. 43-49.

Table 1. Density of samples [22].

Material type	Theoretical density (kg/m^3)	Experimental density (kg/m^3)	Matrix void Content (%)	Weight saving potential
E_0	1189.54	1189.54±0.04	----	----
$E_{20}U$	1135.63	1113.01±3.56	1.99	6.43
$E_{40}U$	1081.72	1057.74±6.48	2.22	11.08
$E_{60}U$	1027.82	1001.49±9.54	2.56	15.81
$E_{20}T$	1151.63	1122.05±3.69	2.57	5.67
$E_{40}T$	1113.72	1062.10±3.70	4.63	10.71
$E_{60}T$	1075.82	1015.75±3.71	5.58	14.61

Table 2. Density and void content of cenosphere/epoxy syntactic foam sandwich composites.

Material type	Theoretical density (kg/m^3)	Experimental density (kg/m^3)	Matrix void content (%)
S_{E0}	1236.93	1225.80±1.09	0.91
$S_{E20}U$	1203.24	1177.97±2.99	2.10
$S_{E40}U$	1169.54	1142.64±5.68	2.30
$S_{E60}U$	1135.86	1105.19±8.24	2.71
$S_{E20}T$	1213.24	1181.69±3.88	2.61
$S_{E40}T$	1188.92	1148.73±4.28	3.38
$S_{E60}T$	1165.86	1112.89±7.17	4.54

Table 3. Critical buckling loads for sandwich composites.

Sandwich type	P_{cr} (N)		% Increase w.r.t SE0 (DTM)
	DTM	MBC	
S_{E0}	370.10±17.42	364.28±5.89	----
$S_{E20}U$	399.17±4.87	392.71±9.18	7.86
$S_{E40}U$	444.00±3.56	438.10±5.91	19.96
$S_{E60}U$	464.27±18.82	459.92±8.08	25.44
$S_{E20}T$	443.83±3.30	437.86±5.64	19.92
$S_{E40}T$	448.17±7.41	442.52±4.62	21.09
$S_{E60}T$	514.43±4.05	509.85±5.29	38.99

Table 4. Comparison of buckling loads of cenosphere/epoxy syntactic foams and their sandwiches [22].

Syntactic foam	P_{cr} (N)		Sandwich type	P_{cr} (N)		% Increase w.r.t syntactic foam (DTM)
	DTM	MBC		DTM	MBC	
E_0	237.67 ± 11.02	231.83 ± 12.51	S_{E0}	370.10 ±17.42	364.28 ± 5.89	55.72
$E_{20}U$	287.58 ± 12.35	281.83 ± 12.85	$S_{E20}U$	399.17 ± 4.87	392.71 ± 9.18	38.81
$E_{40}U$	343.45 ± 14.29	339.33 ± 14.36	$S_{E40}U$	444.00 ± 3.56	438.10 ± 5.91	29.28
$E_{60}U$	387.33 ± 15.04	379.17 ± 17.03	$S_{E60}U$	464.27 ± 18.82	459.92 ± 8.08	19.87
$E_{20}T$	315.50 ± 12.78	306.67 ± 12.52	$S_{E20}T$	443.83 ± 3.30	437.86 ± 5.64	39.79
$E_{40}T$	393.85 ± 16.37	383.83 ± 17.29	$S_{E40}T$	448.17 ± 7.41	442.52 ± 4.62	13.79
$E_{60}T$	479.33 ± 17.76	470.67 ± 16.16	$S_{E60}T$	514.43 ± 4.05	509.85 ± 5.29	7.32

Table 5. Experimental natural frequencies of sandwich beams at no load condition.

Sample Coding	Mode	Natural Frequency (Hz)
S_{E0}	1	212.72
	2	576.26
	3	1123.90
$S_{E20}U$	1	221.47
	2	583.54
	3	1181.90
$S_{E40}U$	1	242.38
	2	611.02
	3	1254.30
$S_{E60}U$	1	246.80
	2	689.94
	3	1285.50
$S_{E20}T$	1	241.98
	2	615.59
	3	1125.00
$S_{E40}T$	1	251.41
	2	620.09
	3	1240.00
$S_{E60}T$	1	261.49
	2	711.71
	3	1323.30

Table 6. Properties of sisal fibres.

Parameter	Value
Young's modulus of Natural fiber (Yarn)	8861.11±138.90 MPa
Strength of the natural fiber (Yarn)	255±8.35MPa
Density of fibre	1262.86±46.21 kg/m^3
Poisson's ratio [47]	0.2

Table 7. Properties of Epoxy matrix.

Property	Value
Density (kg/m^3)	1189.54
Young's Modulus of matrix (GPa)	3.9178
Poisson's ratio of matrix	0.35
Tensile strength (MPa)	36.62
Compressive strength (MPa)	70.74
Flexural Strength (MPa)	70.06
Coefficient of thermal expansion [23] (1/°C)	82×10^{-6}

Table 8. Lamina intrinsic properties and reinforcement geometry.

Property	Value
Volume fraction of fiber	0.4852
Thickness of lamina (mm)	0.75
Number of fibers in wrap and fill direction(1/cm)	6
Average thickness of dry lamina (mm)	0.723
Fill width (mm)	1.667
Fill thickness (mm)	0.32
Gap between tows in fill direction (mm)	0.5
Warp width (mm)	1.667
Warp thickness (mm)	0.32
Gap between tows in warp direction (mm)	0.5
Neat matrix thickness (mm)	0.11
Harness	2
Shift	1
Interlacing	1

Table 9. Comparison of sisal fabric/epoxy laminate properties obtained from CADEC and experimental.

Property	CADEC	Experimental	% difference w.r.t CADEC
Young's Moduli, E_1 (MPa)	6331	6950.01±139	-8.91
Young's Moduli, E_2 (MPa)	6331	5783.33±115	9.47
Poisson's Ratio, υ_{12}	0.252	----	
Poisson's Ratio, υ_{23}	0.252	----	
Shear Moduli, G_{12} (MPa)	2522	----	
Shear Moduli, G_{23} (MPa)	2522	----	

Table 10. Young's modulus of samples predicted using Bardella-Genna model [22].

Sample Type	Young's Modulus (MPa)	Poisson's Ratio
E_0	3917.81	0.35
$E_{20}U$	4541.20	0.317
$E_{40}U$	5258.30	0.284
$E_{60}U$	6100.40	0.251
$E_{20}T$	4898.40	0.317
$E_{40}T$	6137.50	0.284
$E_{60}T$	7712.00	0.251

Table 11. Comparison of experimental and numerically obtained buckling loads of sandwich composites.

Sample Type	Experimental P_{cr} (N)		Numerical P_{cr} (N)		% Difference w.r.t Experimental (DTM)	% Difference w.r.t Experimental (MBC)
	DTM	MBC	DTM	MBC		
S_{E0}	370.10 ±17.42	364.28 ± 5.89	360	355	2.73	2.55
$S_{E20}U$	399.17 ± 4.87	392.71 ± 9.18	368	365	7.81	7.06
$S_{E40}U$	444.00 ± 3.56	438.10 ± 5.91	385	377	13.29	13.95
$S_{E60}U$	464.27 ± 18.82	459.92 ± 8.08	419	410	9.75	10.85
$S_{E20}T$	443.83 ± 3.30	437.86 ± 5.64	383	380	13.7	13.21
$S_{E40}T$	448.17 ± 7.41	442.52 ± 4.62	395	385	11.86	12.99
$S_{E60}T$	514.43 ± 4.05	509.85 ± 5.29	425	416	17.39	18.41

Table 12. Comparison of natural frequency values obtained through experimental and numerical approaches.

Sample Coding	Mode	Natural Frequency (Hz)		% deviation
		Experimental	Numerical	
S_{E0}	1	212.72	205.12	3.57
	2	576.26	581.86	-0.97
	3	1123.90	1187.30	-5.64
$S_{E20}U$	1	221.47	210.75	4.84
	2	583.54	597.48	-2.39
	3	1181.90	1221.40	-3.34
$S_{E40}U$	1	242.38	216.97	10.48
	2	611.02	615.35	-0.71
	3	1254.30	1258.70	-0.35
$S_{E60}U$	1	246.80	223.92	9.27
	2	689.94	644.51	9.44
	3	1285.50	1300.20	-1.14
$S_{E20}T$	1	241.98	211.48	12.6
	2	615.59	599.66	2.59
	3	1125.00	1226.20	-9
$S_{E40}T$	1	251.41	218.99	12.90
	2	620.09	630.73	-1.72
	3	1240.00	1271.40	-2.53
$S_{E60}T$	1	261.49	227.95	12.83
	2	711.71	686.11	3.60
	3	1323.30	1324.80	-0.11

Figure captions

Figure 1. Sandwich preparation steps. 30
Figure 2. Schematic of experimental setup showing buckling and free vibration tests. 30
Figure 3. Sisal yarn tensile test in-progress. 31
Figure 4. Macrostructural geometry of the fabric. 31
Figure 5. Flow chart showing steps of numerical analysis. 31
Figure 6. (a) Untreated (b) treated cenosphere particles and (c) as cast $E_{60}U$ Sample..... 32
Figure 7. (a) Schematic representation of sandwich and (b) prepared sandwich composite. 32
Figure 8. SEM images of sandwich composites indicating (a) top and (b) bottom facing thickness and bonding interfaces. 33
Figure 9. Representative set of compressive load-deflection behavior for sandwich beams with syntactic foam core. 33
Figure 10. Representative images of syntactic foam sandwich beams (a) before and (b) during buckling test. 34
Figure 11. Effect of axial compressive load on natural frequencies of (a) 1^{st} (b) 2^{nd} and (c) 3^{rd} mode. 35
Figure 12. (a) Sisal fibers (b) yarns (c) plain woven fabric and (d) SEM image of dry fabric. 36
Figure 13. Representative stress-strain response for tested yarn. 36
Figure 14. Comparison of load-defection curves obtained experimentally and numerically for (a) $S_{E40}U$ and (b) $S_{E40}T$ sandwich composites. 37

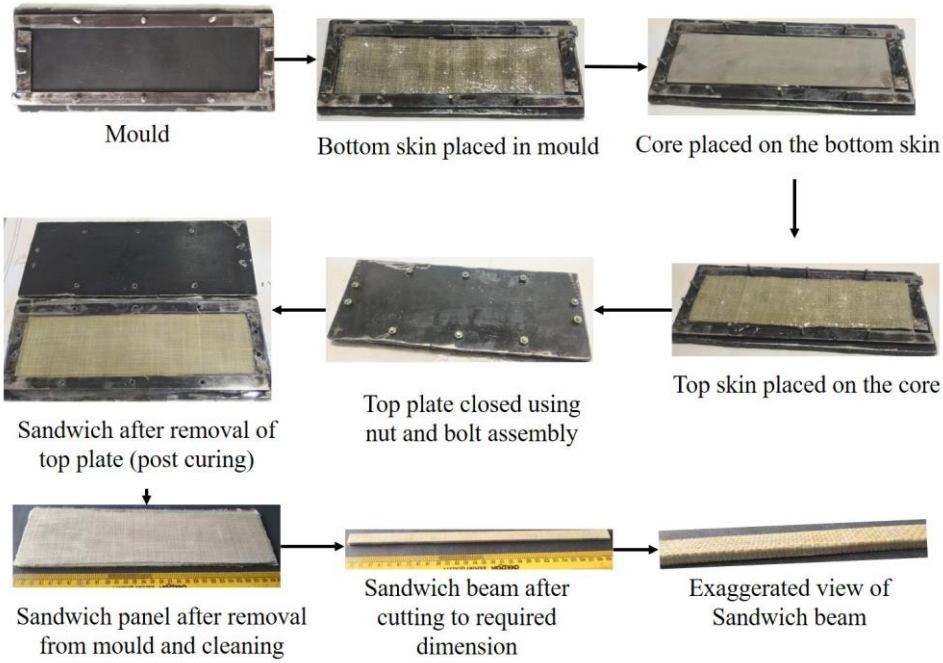

Figure 1. Sandwich preparation steps.

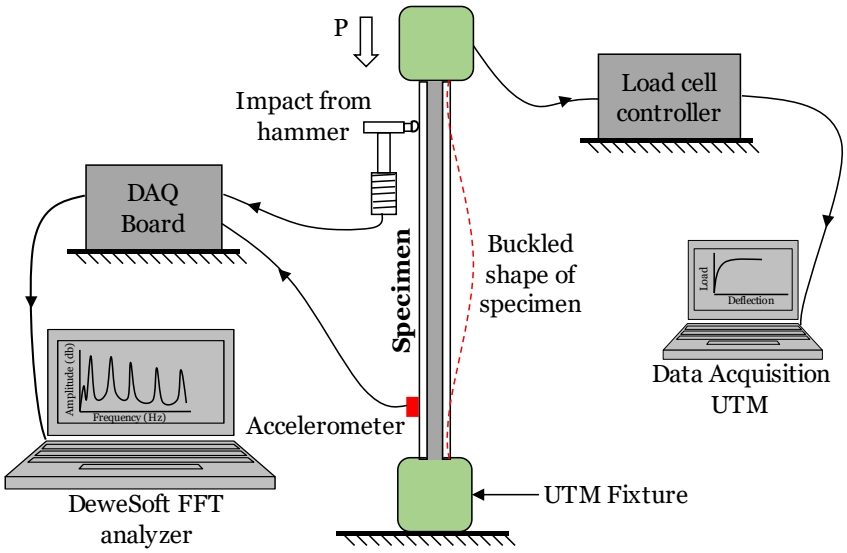

Figure 2. Schematic of experimental setup showing buckling and free vibration tests.

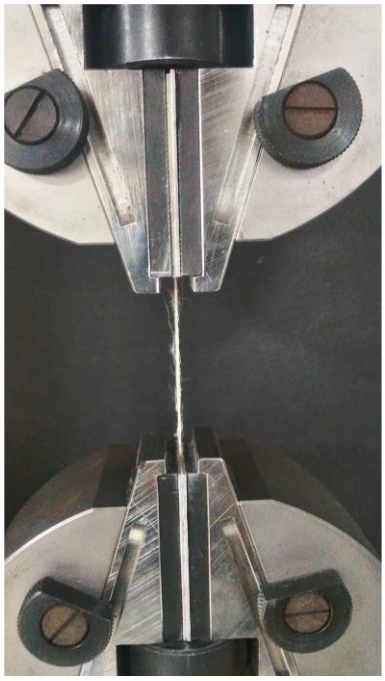

Figure 3. Sisal yarn tensile test in-progress.

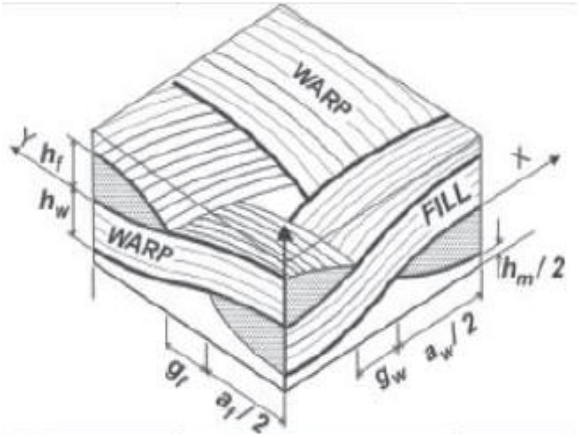

Figure 4. Macrostructural geometry of the fabric.

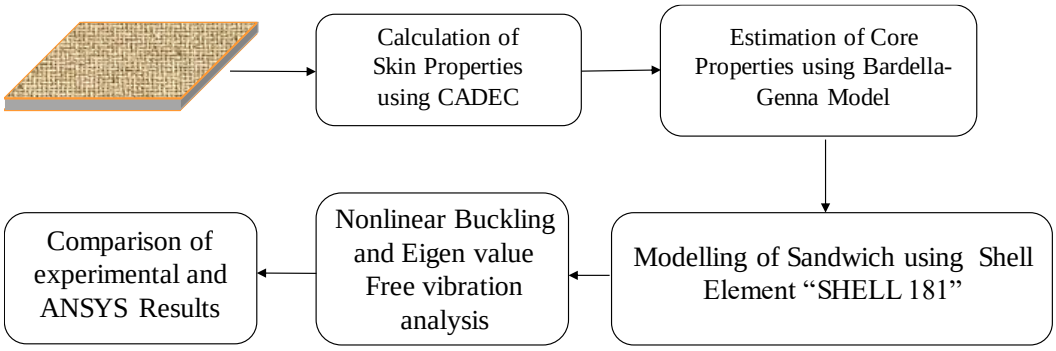

Figure 5. Flow chart showing steps of numerical analysis.

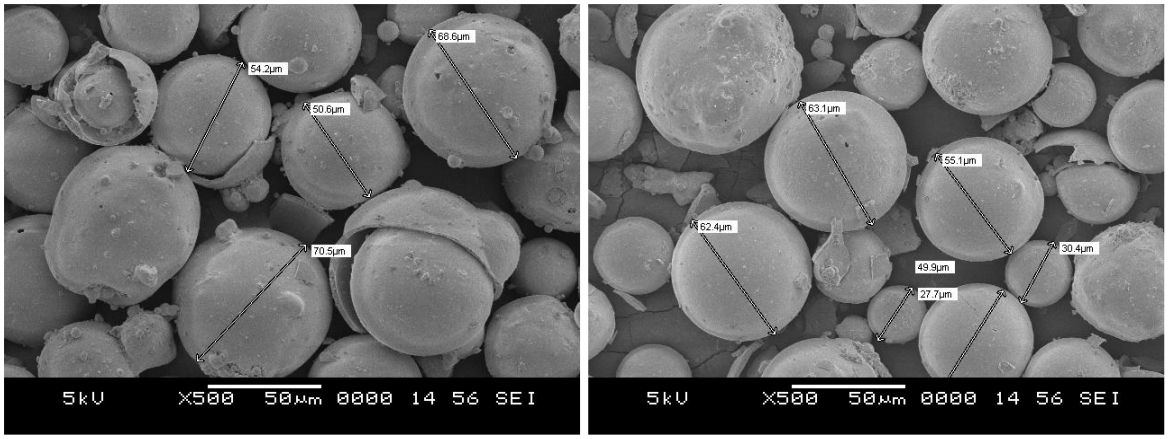

(a) (b)

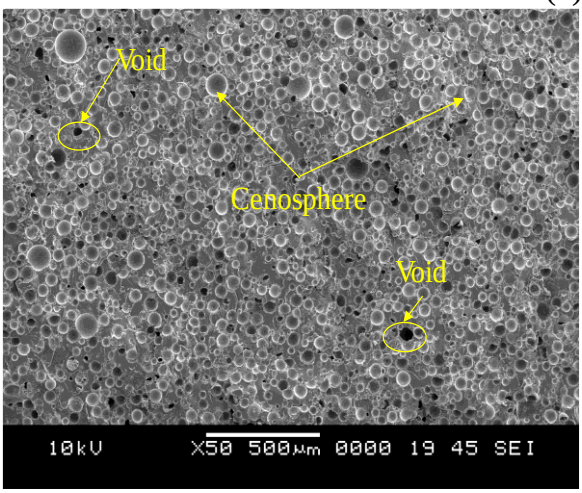

(c)

Figure 6. (a) Untreated (b) treated cenosphere particles and (c) as cast $E_{60}U$ Sample.

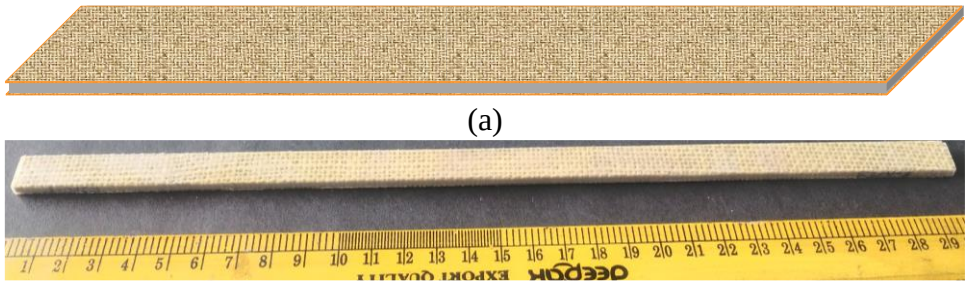

(a)

(b)

Figure 7. (a) Schematic representation of sandwich and (b) prepared sandwich composite.

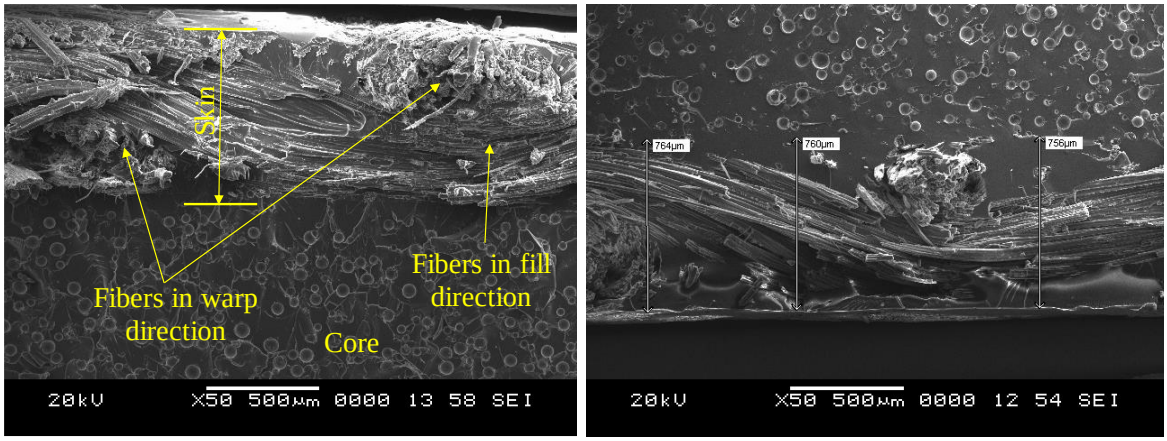

(a) (b)

Figure 8. SEM images of sandwich composites indicating (a) top and (b) bottom facing thickness and bonding interfaces.

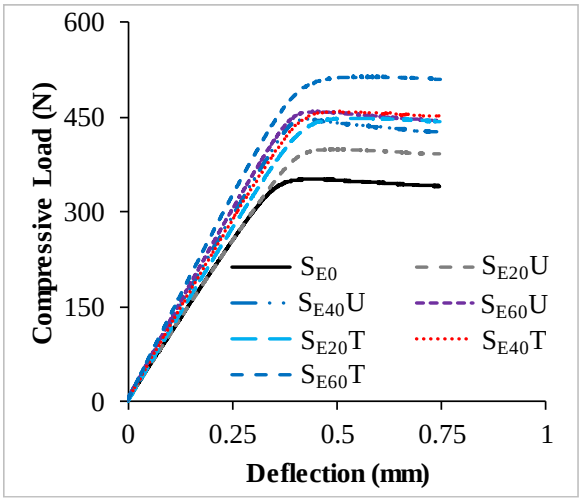

Figure 9. Representative set of compressive load-deflection behavior for sandwich beams with syntactic foam core.

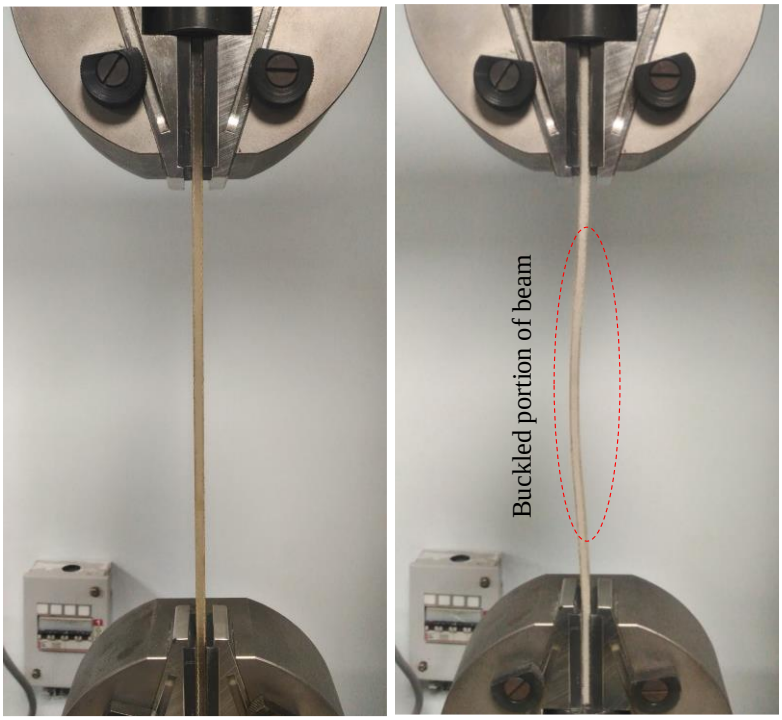

(a) (b)

Figure 10. Representative images of syntactic foam sandwich beams (a) before and (b) during buckling test.

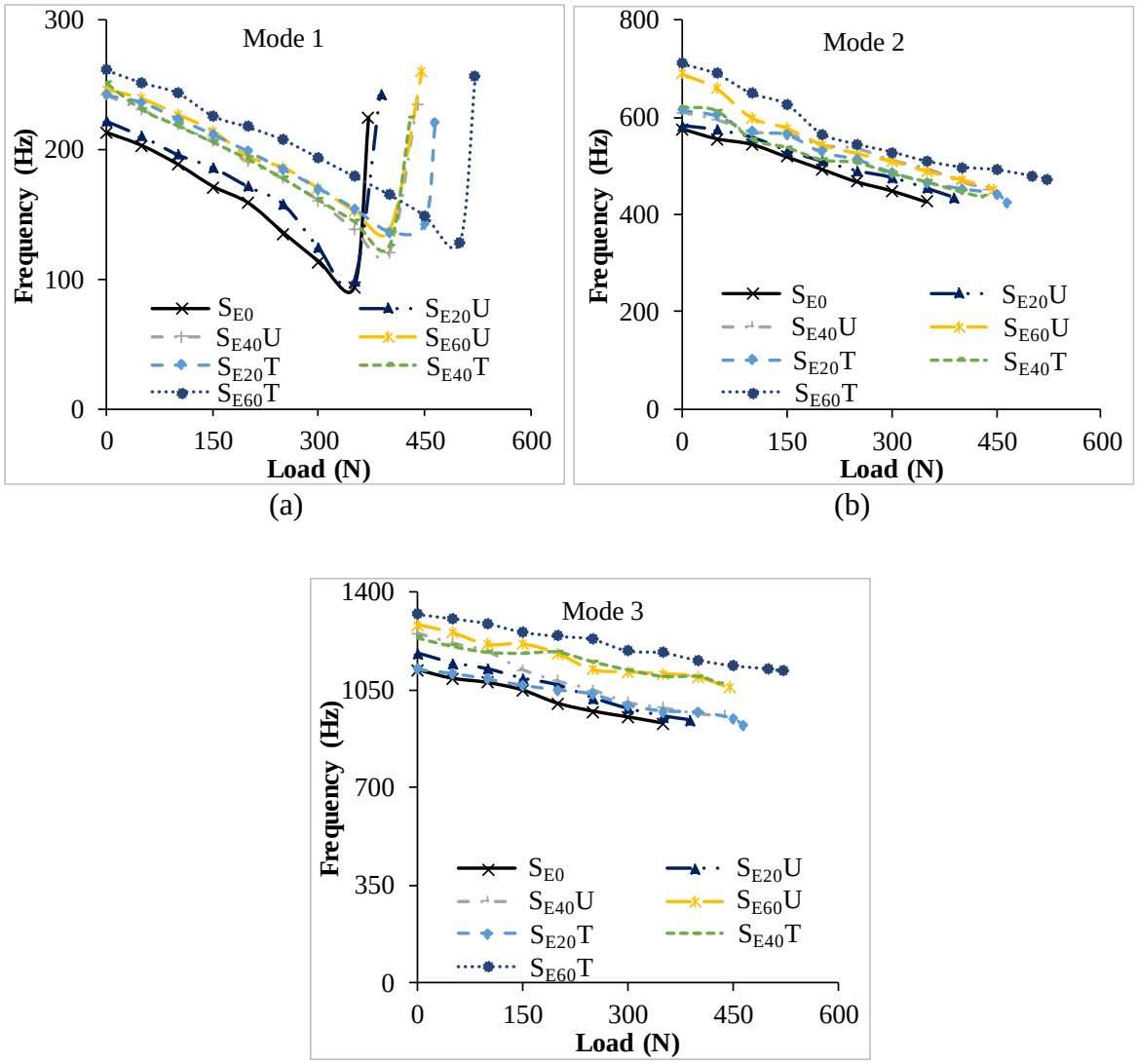

Figure 11. Effect of axial compressive load on natural frequencies of (a) 1st (b) 2nd and (c) 3rd mode.

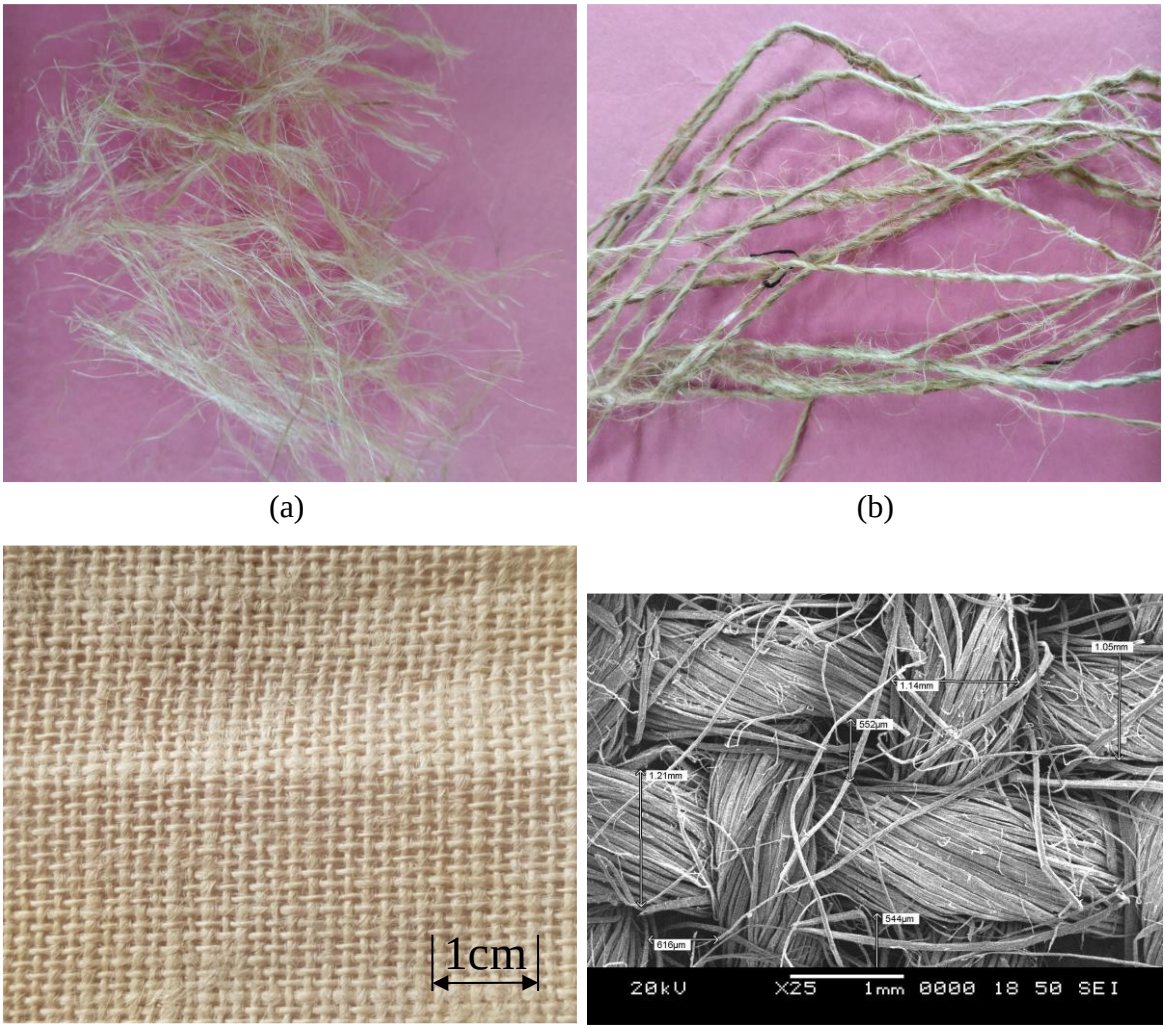

Figure 12. (a) Sisal fibers (b) yarns (c) plain woven fabric and (d) SEM image of dry fabric.

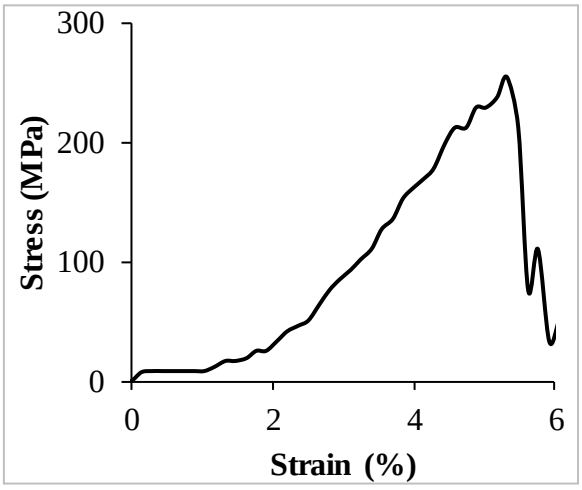

Figure 13. Representative stress-strain response for tested yarn.

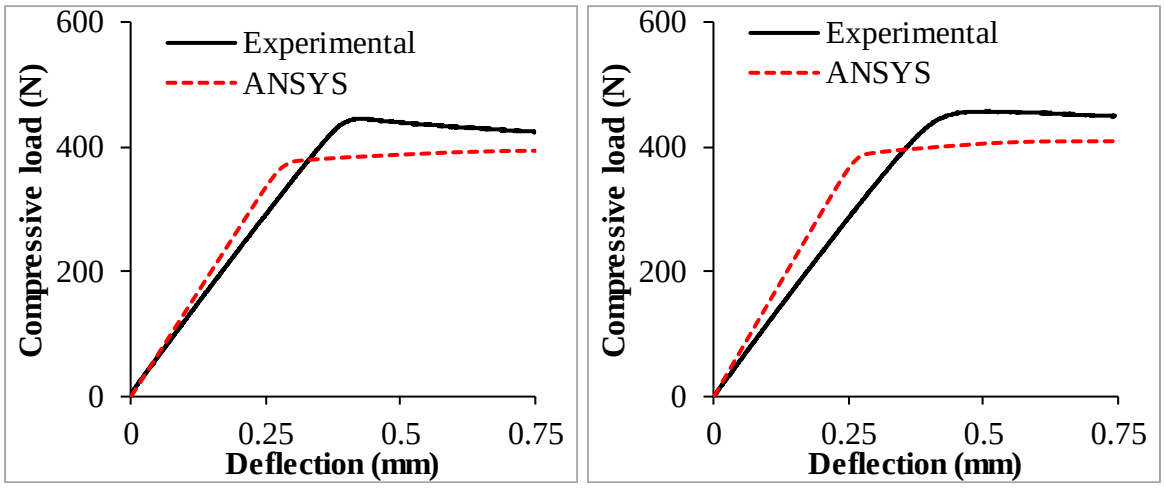

(a) (b)

Figure 14. Comparison of load-defection curves obtained experimentally and numerically for (a) $S_{E40}U$ and (b) $S_{E40}T$ sandwich composites.